Research Article

Engineering: Open Access

Experimental and Numerical Investigation of Flexural Behaviour of GFRP Reinforced Concrete Beams using ANSYS

Kumar Shaswat[1*] and Sneha Gupta[2]

[1]*Department of Civil Engineering, Madan Mohan Malaviya University of Technology, India*

[2]*Assistant Professor, Department of Civil Engineering, Madan Mohan Malaviya University of Technology, India*

[*]Corresponding Author
Kumar Shaswat, Department of Civil Engineering, Madan Mohan Malaviya University of Technology, India.

Submitted: 2025, Mar 14; **Accepted:** 2025, Apr 16; **Published:** 2025, Apr 21

Citation: Shaswat, K., Gupta, S. (2025). Experimental and Numerical Investigation of Flexural Behaviour of GFRP Reinforced Concrete Beams using ANSYS. *Eng OA, 3*(4), 01-18.

Abstract

The construction industry has made extensive use of glass fiber-reinforced polymer (GFRP) rebars to improve structural strength and stop corrosion. High tensile strength-to-weight ratio, non-conductivity, electromagnetic resistance, and robust fatigue resistance are some advantages of GFRP bars. In reinforced concrete projects, GFRP bars are stronger, lighter, and more corrosion-resistant than traditional steel-reinforced bars. This work examines the flexural behaviour of a concrete beam reinforced with GFRP bars by experimental, computational, and analytical methods. Using IS 18256:2023 and IS 456:2000, two 150x150x700 mm GFRP Reinforced Concrete (RC) beams that were doubly-reinforced with 12 mm diameter, 660 mm long GFRP rebars, and 6 mm diameter, 3/4 in steel stirrups were tested under four-point loading conditions in a loading frame with a 40 T capacity. The beam model element type is BEAM188, while the concrete model element type is SOLID65. Nonlinear numerical modelling of GFRP RC beams is done with ANSYS APDL. This study's primary goal is to examine the behaviour of load versus deflection, the mode of failure, and the impact of concrete strength and reinforcement ratio on the crack width of GFRP RC beams. A comparison between the numerical and analytical analysis and the experimental mid-span deflection was made. The experimental results were in agreement with the deflection predicted by the computer analysis. Numerical analysis, codes ACI 440.1R CSA S806, and the suggested approach were used to compare the experimental data. There was a strong correlation between the experimental results and the suggested approach and numerical analysis.

Keywords: Glass Fiber Reinforced Polymer Rebar, Finite Element Analysis, GFRP Reinforced Concrete Beam, Mode of Failure, Deflection

1. Introduction

One composite material that can be utilized as reinforcement for concrete constructions is glass fiber-reinforced polymer (GFRP) bars [1]. Resistance to corrosion, high tensile strength, thermal compatibility, electric and magnetic neutrality, thermal insulation, and lightweight are just a few of the benefits that GFRP bars offer over traditional steel bars [2]. A new option for long-lasting and environmentally friendly concrete buildings is GFRP bars, one major disadvantage of concrete, one of the most used building materials in the world, is that it is weak under tension [3]. Steel bars, which offer tensile strength and ductility, are typically used to reinforce concrete in order to get around this restriction but steel bars can corrode, especially in extreme conditions when they are exposed to moisture, chemicals, and salt, in addition to causing concrete cover cracking and spalling, corrosion weakens reinforced concrete and shortens its service life, thus jeopardizing safety and structural integrity [4]. Researchers and engineers have created a substitute reinforcing material to solve this issue: GFRP bars, the continuous glass fibers that make up GFRP bars are embedded in a polymer resin matrix, which gives them corrosion resistance and a solid concrete bond [5]. Steel bars lack the corrosion resistance, high tensile strength, thermal compatibility, electric and magnetic neutrality, thermal insulation, and lightweight nature of GFRP bars, these characteristics make GFRP bars appropriate for a range of applications where sustainability and durability are needed, including parking buildings, bridges, retaining walls, foundations,

roadways, and slabs, with the GFRP-reinforced bar, numerous experimental flexural behaviour experiments were carried out [6].

An experimental, numerical, and analytical investigation of the flexural behaviour of the concrete beam reinforced with GFRP bars is presented in this research, two 150 x 150 x 700 mm GFRP Reinforced Concrete (RC) beams were evaluated in a loading frame with a 40 T capacity under four-point loading conditions. Investigating the load versus deflection behaviour, mode of failure, and impact of concrete strength and reinforcement ratio on the crack width of GFRP RC beams is the primary goal of this work. Three examples were produced for each of the three sets of concrete beams. Group had M20 concrete strengths (20 MPa) and percentages of reinforcing ratio (0.67%). The type of FRP bars, span-depth ratio, reinforcing ratio, and concrete strength were all examined in the study [7]. Numerical analysis was used in some additional study, optimum analysis study was conducted both experimentally and numerically with GFRP rebars [8-13]. Compared to the steel-reinforced concrete beam, the final load-carrying capability is determined, and deflection is three times greater [14]. The maximum strength of a concrete beam reinforced with GFRP bars coated in sand is also 1.4 to 2.0 times higher than that of a concrete beam reinforced with steel [15,16]. Compare the experimental results with the current theoretical formulae for deflection prediction and the ultimate moment prediction of ACI 440.2R-17, it was discovered that both the mid-span and middle support sections' moment capacities were accurately estimated by the ACI 440.2R-17. Examined flexural behaviour using a four-point loading test, looking at the load-deflection relationship, flexural capacity, stiffness, and mechanism of failure, up to 98% more weight could be supported by concrete beams reinforced with GFRP bars than by those strengthened with steel bars [2,17]. To understand the uses of GFRP reinforcement in flexural members, researchers examined the different characteristics of GFRP-reinforced beams, GFRP-reinforced concrete components may not be ductile according to the standard definitions of ductility because the GFRP bar has a high strength and no yield point [18]. Therefore, in order to comprehend the behaviour of such systems, a thorough investigation is required, the primary goal of the research is to improve the beam's structural performance by utilizing locally accessible materials. The current investigation used a GFRP rebar concrete beam with different concrete grades and reinforcement ratios. The study compared the three groups of concrete beams in terms of the load-deflection reactions, mechanism of failure, and crack breadth. ANSYS software was used to build the Finite Element Model (FEM), a numerical analytical tool, and compare the experimental results with the expected deflection. Results from experiments are more closely correlated with the suggested approach and numerical analysis.

2. GFRP Reinforced Concrete Beam Design (as per IS 456:2000 & IS 18256:2023)

Figure 1: Geometric Details of the Specimens

Loads:

Depth of the beam = 150 mm, Width of the beam = 150 mm, f_y = 415 N/mm^2, f_u = 494 N/mm^2, Self-weight of the beam = 25(0.15)(0.15) = 0.5625 kN/m, Live load = 100 kN/m, Total load = 100.5625 kN/m.

Determine the design shear and design moment:

Design moment: $M_u = wl^2/8 = 150.85x0.7^2/8 = 9.24$ kNm, Design shear force: $V_u = wl/2 = 150.85x0.7/2 = 52.8$ kN.

Determine the limiting MOR for a section of singly reinforced beam:

For Fe415, limiting moment of resistance,

$M_{ulim} = 0.138f_{ck}bd^2$, eff. cover = 40 mm, eff. depth of beam = d = 150-40 = 110 mm.

$M_{ulim} = 0.138x20x150x110^2 = 5$ kNm < M_u (= 9.24 kNm)

Thus, doubly reinforced beam section is required in this design.

Determine how much compression reinforcement is needed:

$\Delta M = M_u - M_{ulim} = (9.24-5)$ kNm = 4.24 kNm

$f_{sc} = 0.0035(X_{ulim}-d')\ Es/X_{ulim} = 0.0035(0.48x110-40)0.52x10^5/0.48x110 = 44.122$ N/mm^2

$0.87f_y = 0.87x415 = 361.05$ N/mm^2

$A_{sc} = M_u - M_{ulim}/f_{sc}(d-d') = 4.24x10^6/361.05(110-40) = 167.76$ mm^2

Number of 12 mm bars required = 167.76//4x12^2 = 1.48 ~ 2 Nos. (say)

Thus, 226.2 mm^2 > 167.76 mm^2 (OK).

Determine how much tension reinforcement is needed:

A_{st2} = The tension bar area for balance $A_{sc} = f_{sc}A_{sc}/0.87f_f = 361.05x167.76/0.87x415 = 167.76$ mm^2

$A_{st1} = A_{stlim} = 0.362f_{ck}bX_{ulim}/0.87f_y = 0.362x20x150x-0.48x110/0.87x415 = 158.82$ mm^2

Alternatively, $p_{tlim} = 41.61(f_{ck}/f_y)(X_{ulim}/d) = 41.61(20/415)(0.48) = 0.9625\%$, $A_{stlim} = 0.9625x150x110/100 = 158.82$ mm^2

$A_{st} = A_{st1} + A_{st2} = 158.82 + 167.76\ mm^2 = 326.58\ mm^2$
Number of 12 mm bars required = 326.58/ π /4x122 = 2.88 ~ 3 Nos. (say)
Thus, 339.29 mm^2 > 326.58 mm^2 (OK)
$p_{t\ provided} = A_{st}x100/bd\% = (339.29x100/150x110)\ \% = 2\%$.

Shear reinforcement design:
Nominal shear stress: $\tau_v = V_u/bd = 52.8/150x110\ N/mm^2 = 3.2\ N/mm^2$
According to IS 456:2000 table 19, the design shear strength of concrete for M20 and 2% pt: (τ_c) = 0.79 N/mm2 < (τ_v) = 3.2 N/mm^2
Thus, shear reinforcement is required in this design.
$V_{us} = (\tau_v - \tau_c)(bd = (3.2\text{-}0.79)150x110\ N = 39.765\ kN$
Using 2-legged 6 mm dia. stirrups,
$A_{sv} = 2x/4x6^2 = 56.55\ mm^2$
$S_v = 0.87f_yA_{sv}d/V_{us} = 0.87(415)56.55x110/39.765x1000 = 56.48$ mm c/c

Maximum spacing of stirrups $\Rightarrow \begin{cases} 0.75d = 0.75(110) = 82.5\ mm\ c/c \\ 300\ mm \end{cases}$ (whichever is less)
2-legged, 6 mm-diameter stirrups @ 80 mm c/c are provided close to the supports, and the spacing can be progressively increased as the beam approaches its mid-span.

Control of deflection:
$(l/d)_{actual} = (700/110)_{actual} = 6.36$
$(l/d)_{max} = (l/d)_{basic} K_t K_c$
$A_{sc} = 226.2\ mm^2$
$p_c = 226.2x100/150x110 = 1.37\%$
$K_t = 0.8$ (The IS 456:2000 figure 4)
$K_c = 1.35$ (The IS 456:2000 figure 5)
$(l/d)_{max} = (l/d)_{basic} K_t K_c = 20x0.8x1.35 = 21.6 > 6.36$ (OK).

MOR: Moment of Resistance:
$A_{st} = 3x\pi/4x122 = 339.29\ mm^2$, $A_{sc} = 2x\pi/4x122 = 226.2\ mm^2$
Now, C = T
$0.36f_cbX_u + (f_{sc}\text{-}f_{cc})A_{sc} = f_{st}A_{st}$
Let $f_{st} = f_{sc} = 0.87f_y$ and neglecting 'f_{cc}'. we have,
$X_u = 0.87f_y(A_{st}\text{-}A_{sc})/0.36f_{ck}b = 0.87x415(339.29\text{-}226.2)/0.36x20x150 = 37.80$ mm
Limiting depth of neutral axis for Fe415, $X^{ulim} = 0.48d = 0.48x110 = 52.8$
$X_u < X_{ulim}$
Section is under-reinforced and assumption of $f_{sc} = f_{st} = 0.87f_y$ is correct
$MOR = M_R = 0.36.f_{ck}.b.X_u.(d\text{-}0.42X_u) + fsc.Asc.(d\text{-}d') = 0.36x20x150x37.8(110\text{-}0.42x37.8) + 0.87x415x\text{-}226.2x(110\text{-}40) = 9.56$ kNm.

Shear Force and Bending Moment:

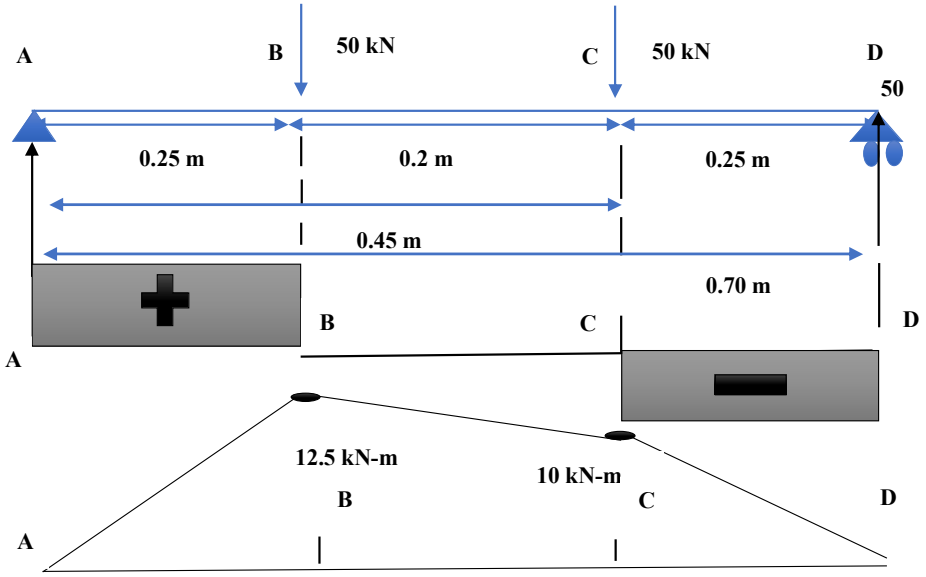

Figure 2: GFRP Beam Support Reactions (SFD & BMD)

$\sum M_A = 0$
50x0.25 + 50x0.45 = RBx0.7
$R_A = R_B = 100/2 = 50$ kN.
BM@A = 50X0 = 0 kNm, BM@B = 50x0.25 = 12.5 kNm, BM@C = (50x0.45) -(50x0.25) = 22.5-12.5 = 10 kNm, BM@D = (50x0.7) -(50x0.45) -(50x0.25) = 35-22.5-12.5 = 0 kNm.

Moment of Inertia:
A = bh = 150x150 = 22500 mm2, = b/2 = 150/2 = 75 mm, = h/2 = 150/2 = 75 mm
$I_x = I_y = bh^3/12 = 150x150^3/12 = 42.1875x10^6\ mm^4$
$I_{xy} = 0$
$I_p = I_x + I_y = bh(h^2+b^2)/12 = 150x150(150^2+150^2)/12 = 84.375x10^6\ mm^4$.

Deflection of Beam:
Reactions:
$\sum M_A = 0$
50x0.25+50x0.45 = RBx0.7
$R_A = R_B = 100/2 = 50$ kN

Consider a section X-X at a distance x from A (in fig.6)

$M_x = 50X/-50(X-0.25)/-50(X-0.45)$

$EId^2y/dx^2 = 50X/-50(X-0.25)/-50(X-0.45)$

$EIdy/dx = 50X^2/2+C1/-50(X-0.25)^2/2/-50(X-0.45)^2/2$

$EI(y) = 50X^3/6+C_1X+C_2/-50(X-0.25)^3/6/-50(X-0.45)^3/6$

Using boundary conditions, at x = 0, y = 0

$0 = 50x0+C_1x0 + C_2-50(0-0.25)^3/6-50(0-0.45)^3/6$

As (X-a) n = $\begin{cases} 0 & X \le a \\ (X-a)^n & X > a \end{cases}$

$0 = 0 + C_1x0 + C_2-0-0$

$C_2 = 0$

At X = 0.7, y = 0

From equation, $0 = 50x0.7^3/6 + C1x0.7-50(0.7-0.25)^3/6-50\ (0.7-0.45)^3/6 = 2.858 + 0.7C_1 - 0.759 - 0.13 = 1.97 + 0.7C_1$

$C_1 = -2.82$

$EIdy/dx = 25X^2 - 2.82/-25(X-0.25)^2/-25(X-0.45)^2$

$EI(y) = 8.34X^3-2.82X+0/-8.34(X-0.25)^3/-8.34(X-0.45)^3$.

(i) Deflection under loads:

Deflection under 50kN load,

X = 0.25 m = 250 mm

Flexural rigidity, $EI = 0.52x10^8x42.1875x10^{-6} = 2193.75\ Nm^2$

$y_c = 1 / EI\ (8.34(0.25)^3 - 2.82x0.25-8.34(0.25 - 0.25)^3 - 8.34(0.25-0.45)^3 = (0.13 - 0.71 - 0 - 0.067) / EI = -0.647/2193.75 = -2.95X10^{-4}$ m = -0.295 mm (Downward)

Deflection under 50 kN load,

X = 0.45 m = 450 mm

$y_D = 1/EI\ (8.34(0.45)^3 - 2.82x0.45-8.34(0.45-0.25)^3 - 8.34(0.45-0.45)^3 = (0.76-1.27-0.067-0)/EI = -0.58/2193.75 = -2.63x10^{-4}$ m = -0.263 mm (Downward).

(ii) Maximum deflection:

For y_{max}, dy/dx = 0

$25X^2 -2.82 - 25(X - 0.25)^2 = 0$

$25X^2 - 2.82 - 25(X^2 + 0.0625 - 0.5X) = 0\ -4.383+12.5X = 0$

X = 0.35 m = 350 mm from end A

y_{max} (at X = 0.35 m) = $1/EI\ (8.34(0.35)^3 - 2.82(0.35) - 8.34(0.35 - 0.25)^3) = -0.64/2193.75 = -2.91x10^{-4}$ m = -0.291 mm (Downward).

Distance of load 100kN from Origin (X) (mm)	Deflection (mm)
250	0.263
350	0.291
450	0.295

Table 1: Details of Theoretical Results

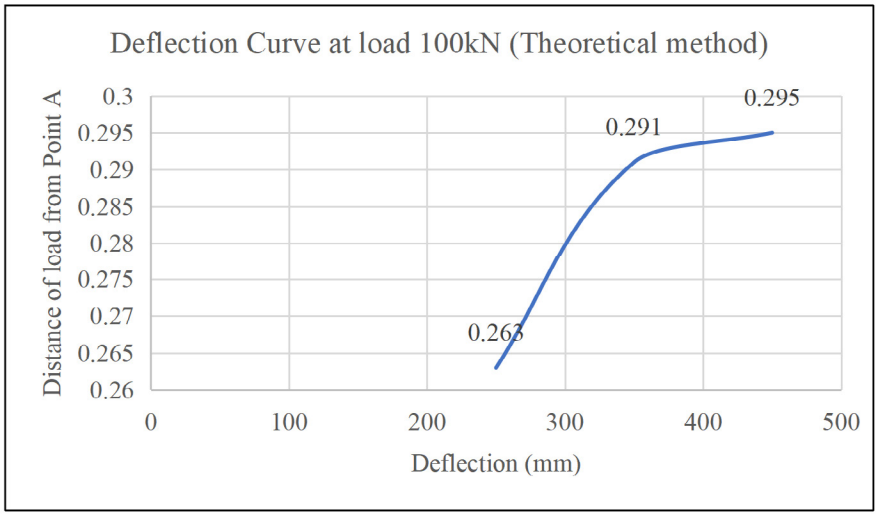

Figure 3: Deflection Curve at Load 100 kN (Theoretical Results)

3. Experimental Program

3.1. Properties of Materials

The M20 grade concrete and 0.67% reinforcing ratio were used in the study of the concrete beam. This study used steel rebar (6 mm) for stirrups and GFRP rebars (12 mm) for tension and compression reinforcement, as seen in Fig. 4(a). The GFRP bars were purchased from SMIN COMPOSITE TECH Pvt Ltd, located in Gurugram's sector 44. A 400 kN capacity Universal Testing Machine (UTM) was used to test all of the GFRP rebars in accordance with the ASTM Standard (ASTM D7205-06), as illustrated in Fig. 4(b). The physical characteristics of the materials are listed in Table 2-6, along with the average findings of the sample's mechanical properties, which included steel rebar, GFRP rebar, and concrete compressive strength.

3.2. Preparation of Specimens

Find the quantities of cement, fine aggregates and coarse aggregates for $0.01575m^3$. The void ratio in cement is 60%, in FA is 40%, and in CA is 44%. Take materials properties are:- Mix is 1:1.5:3 with water-cement ratio of 0.5. One bag of cement weighs 50 kg

(neglecting empty wt. of bag) and density of cement is 1440 kg/m3. Density of FA is 1780 kg/m3 and CA is 1650 kg/m3. Vol. of one bag of cement is 34.7L. Assume vol. of air in concrete as 3% per m3 of concrete.

Vol. of concrete = 0.01575 m^3
Mass of cement in 0.0157 m^3 concrete = x kg
Vol. of air = 3% of vol. of concrete = 0.000471 m^3 = 0.471 mm^3
Vol. of concrete vol. of cement + vol. of FA + vol. of CA + vol. of air + vol. of water
0.0157 = x/2304 + 1.5x/2492 + 3x/2376 + 4.71x10-4 + 0.59x/1000
x = 6.37 kg
Mass of cement in 0.0157 m^3 concrete = x = 6.37 kg
Mass of water = 0.5x = 3.76 kg
Mass of FA = 1.5x = 9.56 kg
Mass of CA = 3x = 19.11 kg. (For 1–Beam)
(For 2-Beams)
Mass of cement = 12.74 kg
Mass of water = 7.52 kg
Mass of FA = 19.12 kg
Mass of CA = 38.22 kg
For 1-Cube
Vol. of concrete = $3.375x10^{-3}$ m3
Mass of cement = x kg
Vol. of air = 3% of vol. of concrete = $1.0125x10^{-4}$ m^3
Vol. of concrete = vol. of cement + vol. of FA + vol. of air + vol. of water
$3.375x10^{-3}$ = x/2304 + 1.5x/2492 + 3x/2376 + $1.0125x10^{-4}$ + 0.5x/1000
x = 1.21 kg
Mass of cement = 1.21 kg
Mass of water = 0.61 kg
Mass of FA = 1.82 kg
Mass of CA = 3.63 kg
For 3-Cubes
Mass of cement = 3.63 kg
Mass of water = 1.83 kg
Mass of FA = 5.46 kg
Mass of CA = 10.89 kg
For 2-Beams + 3-Cubes
Total mass of cement = 16.37 kg
Total mass of water = 9.35 kg
Total mass of FA = 24.58 kg
Total mass of CA = 49.11 kg

The geometric parameters of one set of concrete specimens under study are listed in Table 5. The cross sections of the GFRP rebar concrete beams, which were cast with varying reinforcement ratios, are displayed in Figure 4. There were three steps in the specimen preparation process. 6 mm steel rebar was supplied as two-legged shear reinforcement at 80 mm c/c in the first stage, together with 700 mm long GFRP rebars (12 mm). The OPC 43 M20 grade of concrete was poured into the mould after the GFRP reinforcing cage had been properly aligned on the mould in the second step. To eliminate the voids, the concrete was thoroughly compacted using a vibrator. The specimens were stored for twenty-four hours at room temperature during the third step. The specimens were taken out of the mould and left to cure for 28 days the following day.

3.3. Test Setup

For testing, GFRP-reinforced concrete beams were ready. A 40 T loading frame was used to evaluate the beam. In Figure 3, the experimental setup is displayed. Together, the specimens measured 700 mm in length, with an effective spread of 600 mm. The support was positioned 50 mm from either end of each specimen, with one end hinged and the other end supported by rollers. At an L/3 distance of 200 mm from the support condition, four-point loading was applied to the beam, with 600 mm between the loading sites. The deflection meter was positioned halfway across the beam. For all specimens, the loading rate was kept constant at 0.3 mm/minute until failure. Every beam was subjected to static stress, and for the duration of this experimental investigation, a load increment interval of 2 kN was taken into consideration until the specimens failed.

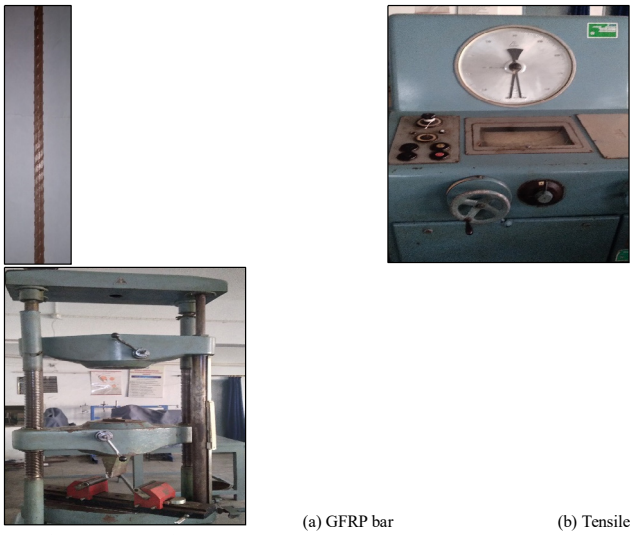

(a) GFRP bar (b) Tensile strength setup for GFRP bar

Figure 4: Details of GFRP Bar

Figure 5: Experimental Setup of the Specimen & Casting of Beam

S.no.	Sample no.	Date of Test	Time of Test	Date of cast	Weight of Sample (kg)	Load (kN)	Compressive Strength (N/mm2)
1	CUBE_1	26-03-2025	03:11:00	27-02-2025	8.43	460.2	20.453
2	CUBE_2	26-03-2025	03:30:00	27-02-2025	8.425	508.8	22.613
3	CUBE_3	26-03-2025	03:42:00	27-02-2025	8.412	567.2	25.208

Table 2: Concrete Cube Compressive Strength Test

Beam	Beam ID	Compressive strength of cubes (MPa)	
Beam_1	B20-1	Target	Tests
		20	20.453
			22.613
			25.208
Beam_2	B20-2	20	20.453
			22.613
			25.208

Table 3: Specimen Designations and Concrete Strength and Material Properties of the Steel and GFRP Bars

Materials	Concrete	GFRP bar (mm) 12	Steel Rebar (mm) 6
Young's modulus (GPa)	31	58	200
Strain (mm/mm)	0.0028	0.0015	0.0020
Poison ratio	0.12	0.33	0.29
Tensile Strength (MPa)	5	493.451	535.26

Table 4: Material Properties of Concrete, Steel and GFRP Bars

Group	Specimen ID	Specimen Details (mm)			GFRP Reinforcement		Tie Reinforcement
		B	D	L	Bottom	Top	
1	B20_1	150	150	700	2#12mm	3#12 mm	#6mm @ 80mm c/c
	B20_2	150	150	700	2#12mm	3#12 mm	#6mm @ 80mm c/c

Table 5: Geometric Details of Specimens

S.no.	Sample no.	Date of Test	Time of Test	Date of cast	Weight of Sample (kg)	Peak Load (kN)	Flexural Strength (N/mm2)	Sample Break Length (mm)
1	BEAM_1	26-03-2025	04:32:00	27-02-2025	38.12	37.86	6.625	269
2	BEAM_2	26-03-2025	04:58:00	27-02-2025	36.43	26.91	4.71	242

Table 6: GFRP Beam Flexural Strength Test Results

4. Results and Discussion

4.1. Behavior of Load-deflection

Figure 12 displays one set of load-deflection curves from the experimental investigation that looked at the load-deflection behaviour of GFRP-reinforced concrete beams. The group-1, B20-1 specimen has a larger ultimate load and a lesser deflection than the B20-2 specimen. Specimen B20-1's ultimate load was 28.94% higher than that of specimen B20-2. The B20-1 specimen has a lower mid-span deflection than the B20-2 specimen. A single group of specimens' load-deflection responses are shown in Figure 12. After reaching the maximal load, the specimens rapidly failed with extensive cracks, as seen in Figure 9. Similarly, after achieving the ultimate load, Figs. 6–11 show that the GFRP RC beam gradually failed with little cracks. In order to improve the concrete's strength and the proportion of steel reinforcement, the examples gradually failed with little cracks.

4.2. Mode of Failure

For the all-concrete beams, the midspan deflection was measured during the experimental research. Increasing the ratio of reinforcement to concrete strength was found to decrease deflection in the experimental study. As shown in Table 5-6, two specimens experienced flexural failure, and concrete crushing was a frequent failure mode in the concrete beams. The specimen's bottom tension zone experienced the greatest failure. The examples B20-1 and B20-2 exhibited the early, final, and failure cracks, as seen in Fig. 6-11.

4.3. Effect of Concrete Strength and Reinforcement Ratio on Crack Width

The crack width of the concrete beams is influenced by the reinforcing ratio and the concrete's compressive strength, as illustrated in Fig. 6-11. For specimens B20-1 and B20-2, the initial crack width was 0.122 and 0.10 mm, respectively, under an initial load of 9.8 kN. As demonstrated in an experimental investigation in Fig. 11, the fracture width decreases with increasing concrete's compressive strength and reinforcing ratio. The final crack widths for specimens B20-1 and B20-2 are 0.769 mm and 0.688 mm, respectively.

Figure 6: Beam-1 First Stage Deflection at Load 9.8 kN

1. BEAM_1	Load (kN)	Deflection (mm)
Experimental result	9.8	0.122A

Table 7: Details of Beam-1 First Stage Deflection at Load 9.8 kN

Figure 7: Beam-1 Second Stage Deflection at Load 19.2 kN

2. BEAM_1	Load (kN)	Deflection (mm)
Experimental result	19.62	0.225

Table 8: Details of Beam-1 Second Stage Deflection at Load 19.62 kN

Figure 8: Beam-1 Third Stage Deflection at Load 24.52 kN

3. BEAM_1	Load (kN)	Deflection (mm)
Experimental result	24.52	0.356

Table 9: Details of Beam-1 third stage deflection at load 24.52 kN

Figure 9: Beam-1 Fourth Stage Deflection at Load 29.42 kN

4. BEAM_1	Load (kN)	Deflection (mm)
Experimental result	29.42	0.463

Table 10: Details of Beam-1 Fourth Stage Deflection at Load 29.42 kN

Figure 10: Beam-1 Fifth Stage Deflection at Load 34.33 kN

5. BEAM_1	Load (kN)	Deflection (mm)
Experimental Result	34.33	0.582

Table 11: Details of Beam-1 Fifth Stage Deflection at Load 34.33 kN

Figure 11: Beam-1 Sixth stage deflection at load 37.26 kN

6. BEAM_1	Load (kN)	Deflection (mm)
Experimental Result	37.26527	0.769

Table 12: Details of Beam-1 Sixth Stage Deflection at Load 37.26 kN

Load (kN)	**Deflection (mm)**
0	0
9.8	0.122
19.62	0.225
24.52	0.356
29.42	0.463
34.33	0.582
37.86326226	0.769

Table 13: Experimental Results – Load vs. Deflection Details

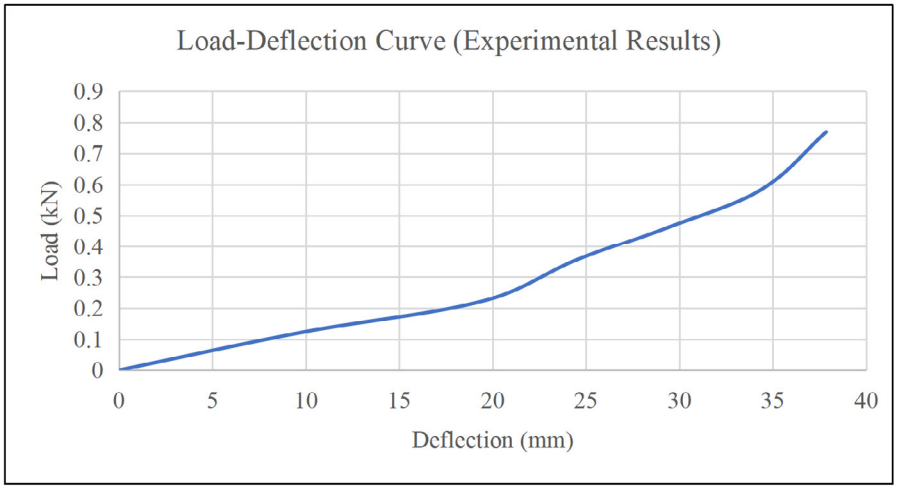

Figure 12: Experimental Result – Load-deflection Graph

5. Numerical Analysis

5.1. Finite Element Model (FEM)

The ANSYS program was used to create the finite element model. The flexural behaviour of GFRP RC beams was investigated using FEA. The load–deflection, initial, ultimate, and failure load, as well as the maximum deflection, were all included in the FEA analysis. In this investigation, four-point loading was used, and Fig. 13-23 shows the FEM.

5.2. Mesh Convergence Study

In this work, the ideal mesh size for this finite element analysis of the beam is shown in Fig. 13-23, which was determined through a mesh convergence investigation. This can help guarantee the accuracy and dependability of the analysis's findings. The mesh size of 30 mm was selected based on the results of the sensitivity analysis. The experimental outcomes may be predicted with the use of this mesh size, which provides a good correlation.

Figure 13: Beam-1 First Stage Deflection at Load 1 kN

1. BEAM_1	Load (kN)	Deflection (mm)
ANSYS Result	1	0.022

Table 14: Details of Beam-1 First Stage Deflection at Load 1 kN

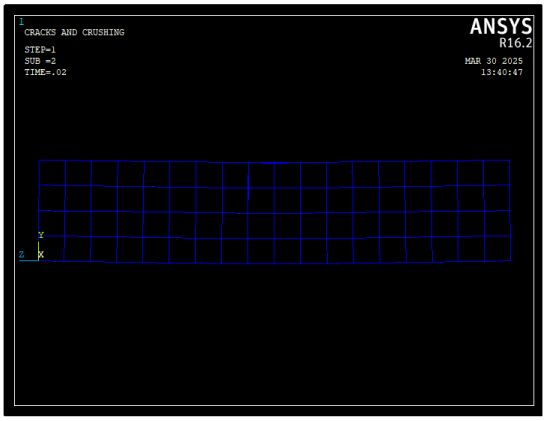

Figure 14: Beam-1 Second Stage Deflection at Load 2 kN

2. BEAM_1	Load (kN)	Deflection (mm)
ANSYS Result	2	0.043

Table 15: Details of Beam-1 Second Stage Deflection at Load 2 kN

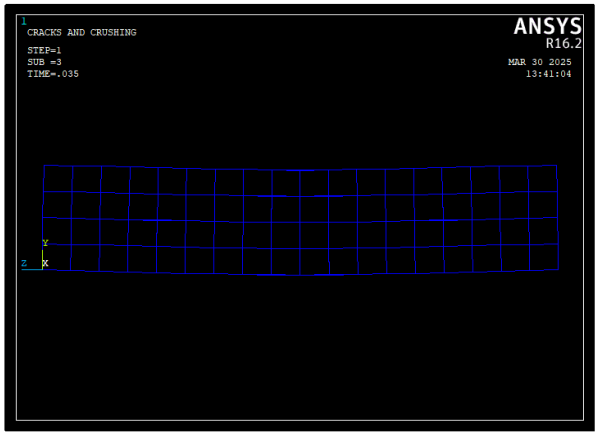

Figure 15: Beam-1 Third Stage Deflection at Load 3.5 kN

3. BEAM_1	Load (kN)	Deflection (mm)
ANSYS Result	3.5	0.075

Table 16: Details of Beam-1 third stage deflection at load 3.5 kN

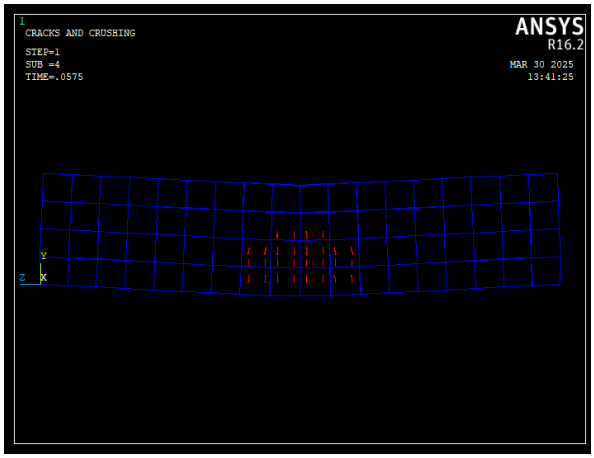

Figure 16: Beam-1 Fourth Stage Deflection at Load 5.75 kN

4. BEAM_1	Load (kN)	Deflection (mm)
ANSYS Result	5.75	0.166

Table 17: Details of Beam-1 Fourth Stage Deflection at Load 5.75 kN

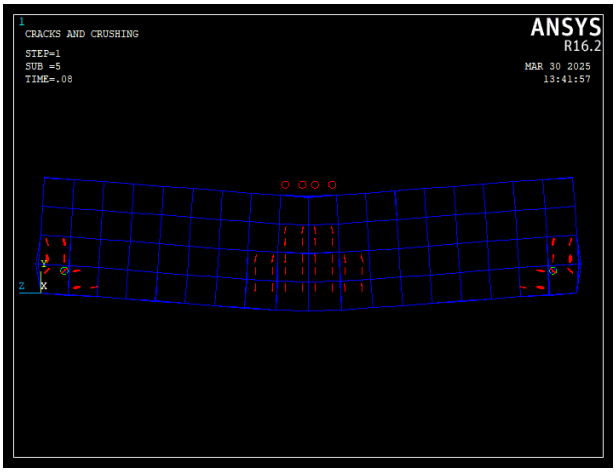

Figure 17: Beam-1 Fifth Stage Deflection at Load 8 kN

5. BEAM_1	Load (kN)	Deflection (mm)
ANSYS Result	8	0.248

Table 18: Details of Beam-1 Fifth Stage Deflection at Load 8 kN

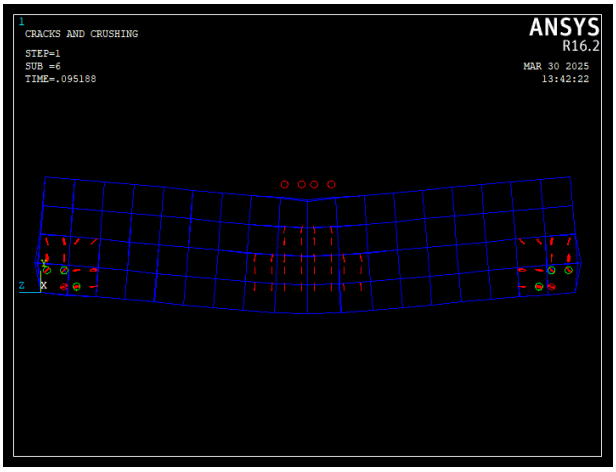

Figure 18: Beam-1 Sixth Stage Deflection at Load 9.519 kN

6. BEAM_1	Load (kN)	Deflection (mm)
ANSYS Result	9.519	0.297

Table 19: Details of Beam-1 Sixth Stage Deflection at Load 9.519 kN

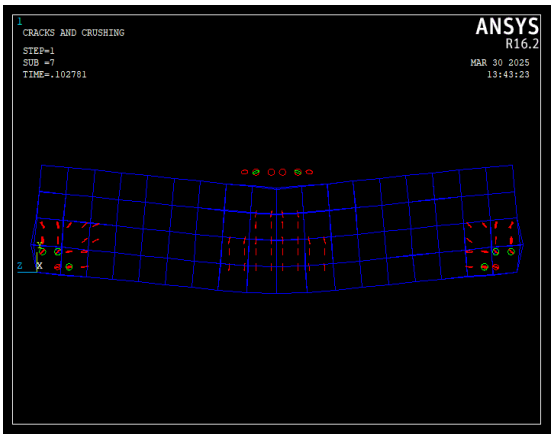

Figure 19: Beam-1 Seventh Stage Deflection at Load 10.278 kN

7. BEAM_1	Load (kN)	Deflection (mm)
ANSYS Result	10.278	0.322

Table 20: Details of Beam-1 Seventh Stage Deflection at Load 10.278 kN

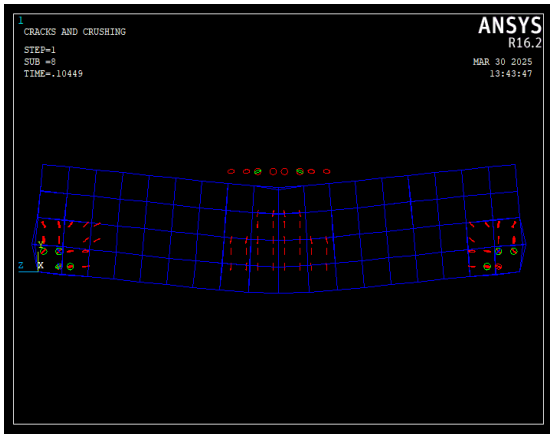

Figure 20: Beam-1 Eighth Stage Deflection at Load 10.449 kN

8. BEAM_1	Load (kN)	Deflection (mm)
ANSYS Result	10.449	0.329

Table 21: Details of Beam-1 Eighth Stage Deflection at Load 10.449 kN

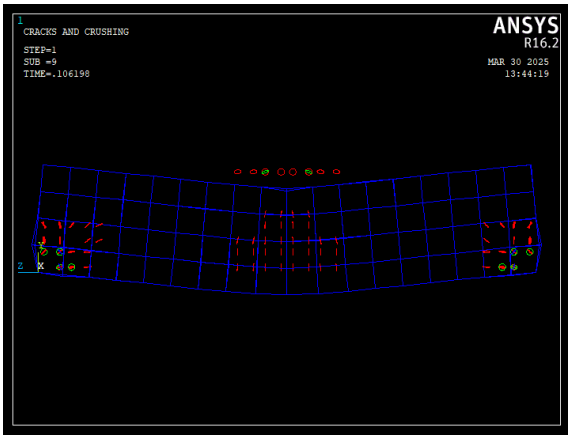

Figure 21: Beam-1 Ninth Stage Deflection at Load 10.62 kN

9. BEAM_1	Load (kN)	Deflection (mm)
ANSYS Result	10.62	0.341

Table 22: Details of Beam-1 Ninth Stage Deflection at Load 10.62 kN

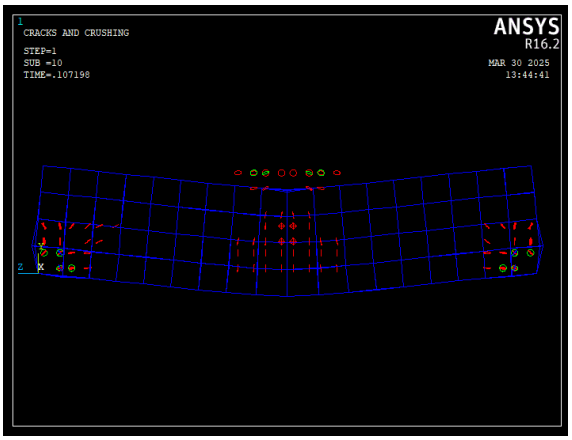

Figure 22: Beam-1 Tenth Stage Deflection at Load 10.72 kN

10. BEAM_1	Load (kN)	Deflection (mm)
ANSYS Result	10.72	0.343

Table 23: Details of Beam-1 Tenth Stage Deflection at Load 10.72 kN

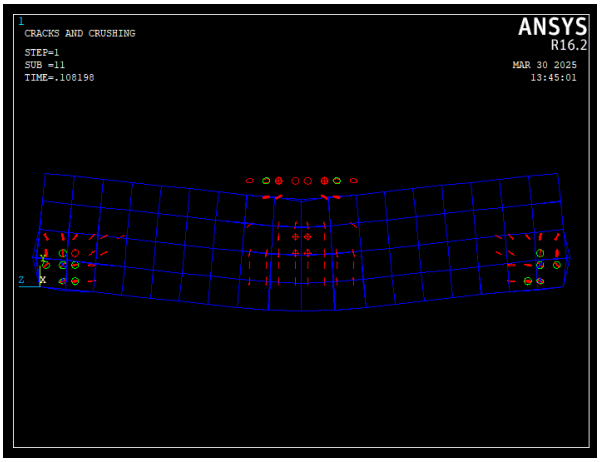

Figure 23: Beam-1 Eleventh Stage Deflection at Load 10.82 kN

11. BEAM_1	Load (kN)	Deflection (mm)
ANSYS Result	10.82	0.353

Table 24: Details of Beam-1 Eleventh Stage Deflection at Load 10.82 kN

Load (kN)	**Deflection (mm)**
0	0
1	0.022
2	0.043
3.5	0.075
5.75	0.166
8	0.248
9.519	0.297

10.278	0.322
10.449	0.329
10.62	0.341
10.72	0.343
10.82	0.353

Table 25: ANSYS Results – Load vs. Deflection Details

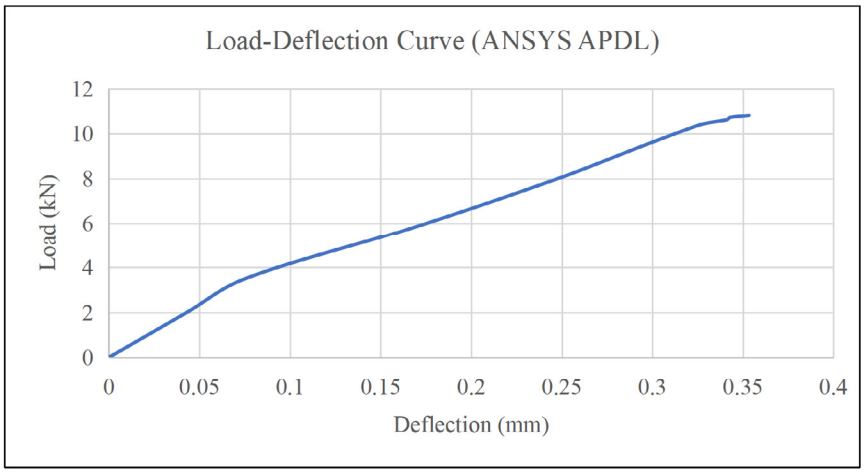

Figure 24: ANSYS Result – Load-deflection Graph

5.3. Comparison of Experimental Study and Numerical Analysis Load–Deflection Responses

Table 25 presents the experimental data that were compared with the numerical analysis. Concrete crushing and flexural collapse caused the majority of the concrete beams to break. As the starting load grew, so did the shear and vertical cracks, which persisted until the ultimate load. Figure 13-23 shows the group specimens' numerical deflection model. In addition to comparing the experimental and numerical results, the ultimate load, failure load, and deflection were shown. The first and failure cracks' experimental and numerical analyses are shown in Figures 6-11 and 13-23. Coefficient of Variation (CV) in experimental and numerical analysis was 0.65% for failure load and 0.90% for ultimate load.

In this study, a 3D model was created and ANSYS APDL software was used to conduct numerical analysis on GFRP RC beams, taking into account load, deflection, and mode of failure. Comparing the experimental ultimate load and deflection data with the numerical ultimate load and deflection values shown in Figure 24 revealed a strong correlation and excellent agreement. For the ultimate load, the corresponding mean, standard deviation, and coefficient of variation are 0.99, 0.01 and 0.90. Similarly, the ultimate deflection has a mean of 0.97, a standard deviation of 0.01 and a coefficient of variation of 0.65.

Experimental Results		**ANSYS Results**	
Load (kN)	Deflection (mm)	Load (kN)	Deflection (mm)
0	0	0	0
9.8	0.122	1	0.022
19.62	0.225	2	0.043
24.52	0.356	3.5	0.075
29.42	0.463	5.75	0.166
34.33	0.582	8	0.248
37.86326226	0.769	9.519	0.297
		10.278	0.322
		10.449	0.329
		10.62	0.341
		10.72	0.343
		10.82	0.353

Table 26: Comparison of Experimental and ANSYS Results – Load vs. Deflection Details

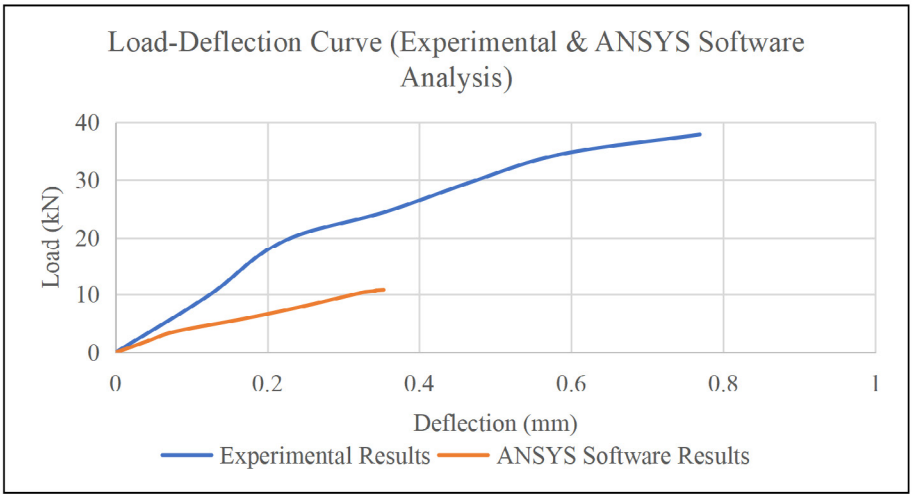

Figure 25: Comparison of Experimental and ANSYS Results – Load-deflection Graph

6. Analytical Study for Deflection Calculation

6.1. Deflection Approach for Current Design Codes

Equation (1) is used to compute the effective moment of inertia based on Branson's method. Branson's method was adjusted to take into consideration the impact of the moment of inertia in light of experimental findings [19]. Modified Eq. (2) incorporates the GFRP rebars' modulus of elasticity, bond characteristics, and reduction coefficient [20].

$$l_e = l_g\,(M_{cr}/M_a)^3 + l_{cr}(1 - M_{cr}/M_a)^3 \le l_g \quad (1)$$

where:

$M_{cr} = (f_r/f_{rb})$

$f_r = 0.6\sqrt{f_c}$

$$\beta_d = 1/5(\rho_f/\rho_{fb}) \le 1.0 \quad (2)$$

where l_e is the effective moment of inertia, l_g is the effective moment of inertia of the gross section, and l_{cr} is the effective moment of inertia cracking the transferred concrete area. M_{cr}, M_a,f_c and f_r are referred to as cracking moment, service moment, compressive strength of concrete and modulus of rupture.

6.2. Proposed Method

The theoretical and effective moment of inertia is computed using Equations (3) and (4) based on the earlier equations. Eq. (5) provides the actual and balanced ratio that was used to derive the modification factor βd. To determine the coefficient of X_1 and X_2 values, experimental load-deflection data were utilized.

$$(I_e)_{exp} = P_{exp} L_a/48E_c\,\delta_{exp}\,(3L^2\text{-}4L_a^2) \quad (3)$$

$$(l_e)_{Theo} = \beta_d\,(M_{cr}/M_a)^3\,l_g + X_2\,(1\text{-}M_{cr}/M_a)^3)\,l_{cr} \le l_g \quad (4)$$

$$\beta_d = X_1\,(\rho_f/\rho_{fb}) \le 1.0 \quad (5)$$

where: E_c is the modulus of elasticity of the concrete, is the mid-span deflection of the specimens, and L and L_a is the total and effective length of the specimen. ρf and ρf_b are referred to as actual and balanced reinforcement ratios. β_d is the modification factor.

6.3. Evaluation of the Proposed Method

Comparisons were made between the experimental results and the suggested techniques (CSA S806-02 and ACI 440.1R-06). Table 26 reports on the numerical analysis. Using Eqs. (3) and (4), the theoretical and effective moment of inertia were computed. As the mean, standard deviation, and coefficient of variation are 0.98, 0.02, and 2.12%, respectively, the experimental mid-span deflection matched the suggested approach. Likewise, there was a strong correlation between the experimental data and the numerical analysis: the mean, standard deviation, and coefficient of variation are 0.97, 0.01 and 1.18%, respectively. Both ACI 440.1R-06 and CSA S806-02 projected the mid-span deflection. Their averages are 0.99 and 1.00. In addition to the coefficient of variation values of 3.94% and 4.59%, the standard deviation values are 0.04 and 0.05. According to the suggested mid-span deflection deviation and experimental codes, 10% was noted.

5. Conclusions and Recommendation

This research used experimental and analytical methods to investigate the flexural behaviour of GFRP-reinforced concrete beams. The experimental tests were conducted using M20 concrete grade beams with reinforcing ratios of 0.67%. The analytical results were validated by comparing them with the experimental deflections. The following are the study's main conclusions:

1. The GFRP concrete beams were examined using a concrete grade of 20 MPa and a reinforcement ratio of 0.67 percent, respectively. The concrete crushing and flexural failure behaviour of all GFRP concrete beams was identical.

2. Raising the concrete grade and reinforcing ratio improved the GFRP RC beams' load-carrying capability.

3. At ultimate load, the concrete beams' crack width is decreased by the following percentages for each specimen: 5.86% for B20-2 and 3.98% for B20-1.

4. The ultimate and failure load prediction coincided with the testing data after comparing them with the numerical analysis. The ultimate load's mean, standard deviation, and coefficient of variation were 0.99, 0.01, and 0.90%, while the failure loads were 0.98, 0.01, and 0.61%.

5. Four approaches were used to estimate the deflection of the concrete beams: numerical analysis, CAS S806, ACI 440.1R, and the suggested method. Neither the CAS S806 nor the ACI 440.1R procedures yielded deflections that matched the experimental findings. Conversely, the suggested approach and numerical analysis produced deflections that nearly matched the outcomes of the experiment. The CV values for these investigations were 3.94%, 4.59%, 2.12%, and 1.18%, in that order.

6. The M20 concrete cube's compressive strength test results are 20.453 N/mm^2, 22.613 N/mm^2, and 25.208 N/mm^2, which indicates that the outcome is satisfactory.

7. At peak loads of 37.86 kN and 26.91 kN, respectively, the flexural strength test values for M20 concrete GFRP beams are 6.63 N/mm^2 and 4.71 N/mm^2, which are acceptable.

8. The finite element model's centerline deflections, stresses, and initial and progressive cracking closely match theoretical data from a GFRP reinforced concrete beam.

9. The failure mechanism of a GFRP reinforced concrete beam is well modelled by FEA, as evidenced by the failure load predicted by FEA being very close to the failure load determined during theoretical calculations.

10. The load delivered at failure closely resembles manually computed results, therefore a finite element software is an excellent tool for predicting the flexural failure of GFRP reinforced concrete beams.

The current study investigated the flexural behaviour of GFRP bars under four-point loads using M20 OPC 43 concrete grade. Additionally, research on introducing fibers and other loading situations will continue.

Acknowledgement

Under the direction of Dr. Sneha Gupta, this study was conducted. I am incredibly appreciative of the advice, expertise, comprehension, and many hours spent assisting me in finishing this research.

References

1. Hassanpour, S., Khaloo, A., Aliasghar-Mamaghani, M., & Khaloo, H. (2022). Effect of compressive glass fiber-reinforced polymer bars on flexural performance of reinforced concrete beams. *ACI Structural Journal, 119*(6), 5-18.
2. Kinjawadekar, T. A., Patil, S., & Nayak, G. (2023). A critical review on glass fiber-reinforced polymer bars as reinforcement in flexural members. *Journal of The Institution of Engineers (India): Series A, 104*(2), 501-516.
3. Sasikumar, P., & Manju, R. (2024). Flexural behaviour of reinforced concrete beams reinforced with Glass Fibre Reinforced Polymer (GFRP) bars: experimental and analytical study. *Asian Journal of Civil Engineering, 25*(4), 3623-3636.
4. Chitsazan, I., Kobraei, M., Jumaat, M. Z., & Shafigh, P. (2010). An experimental study on the flexural behavior of FRP RC beams and a comparison of the ultimate moment capacity with ACI. *Journal of civil engineering and construction technology, 1*(2), 27-42.
5. Dowell, R. K., Ferretti, F., Mazzotti, C., & Faraone, G. (2023, June). Modelling of Reinforced Concrete Columns with GFRP Rebar. In *International Symposium of the International Federation for Structural Concrete* (pp. 151-160). Cham: Springer Nature Switzerland.
6. Feng, R., Chen, Y., Wei, J., Huang, J., Huang, J., & He, K. (2018). Experimental and numerical investigations on flexural behaviour of CFRP reinforced concrete-filled stainless steel CHS tubes. *Engineering Structures, 156*, 305-321.
7. Barris, C., Torres, L., Turon, A., Baena, M., & Catalan, A. (2009). An experimental study of the flexural behaviour of GFRP RC beams and comparison with prediction models. *Composite Structures, 91*(3), 286-295.
8. Kazemi, M., Madandoust, R., Chastre, C., Esfahani, M. R., & Courard, L. (2021, December). Numerical study on the flexural behaviour of normal-and high-strength concrete beams reinforced with GFRP bar, using different amounts of transverse reinforcement. In *Structures* (Vol. 34, pp. 3113-3124). Elsevier.
9. Shen, X., Li, B., Shi, W., & Chen, Y. T. (2022). Numerical study on flexural behaviour of FRP reinforced concrete beams with compression yielding blocks. *Case Studies in Construction Materials, 17*, e01169.
10. Kaveh, A. (2013). *Optimal analysis of structures by concepts of symmetry and regularity* (p. 463). New York: Springer.
11. Kaveh, A., Rahami, H., & Shojaei, I. (2020). *Swift analysis of civil engineering structures using graph theory methods*. Springer International Publishing.
12. Ramesh, B., Eswari, S., & Sundararajan, T. (2021). Experimental and numerical studies on the flexural behaviour of GFRP laminated hybrid-fibre-reinforced concrete (HFRC) beams. *Innovative Infrastructure Solutions, 6*, 1-13.
13. Xingyu, G., Yiqing, D., & Jiwang, J. (2020). Flexural behavior investigation of steel-GFRP hybrid-reinforced concrete beams based on experimental and numerical methods. *Engineering Structures, 206*, 110117.
14. Kabashi, N., Avdyli, B., Krasniqi, E., & Këpuska, A. (2020). Comparative approach to flexural behavior of reinforced beams with GFRP, CFRP, and steel bars. *Civil Engineering Journal, 6*(1), 50-59.
15. Balendran, R. V., Tang, W. E., Leung, H. Y., & Nadeem, A. (2004, August). Flexural behaviour of sand coated glass-fiber reinforced polymer (GFRP) bars in concrete. In *29th Conference on "Our World in Concrete & Structures*.
16. Almahmood, H., Ashour, A., & Sheehan, T. (2020). Flexural behaviour of hybrid steel-GFRP reinforced concrete

continuous T-beams. *Composite Structures, 254*, 112802.
17. Sirimontree, S., Keawsawasvong, S., & Thongchom, C. (2021). Flexural behavior of concrete beam reinforced with GFRP bars compared to concrete beam reinforced with conventional steel reinforcements. J*ournal of Applied Science and Engineering, 24*(6), 883-890.
18. Arinaitwe, D. N. (2020). *Investigation of Flexural Strength of Reinforced Concrete Beams in Rwanda* (Doctoral dissertation, JKUAT-COETEC).
19. Alsayed, S. H., Al-Salloum, Y. A., & Almusallam, T. H. (2000). Performance of glass fiber reinforced plastic bars as a reinforcing material for concrete structures. *Composites Part B: Engineering, 31*(6-7), 555-567.
20. Yost, J. R., Gross, S. P., & Dinehart, D. W. (2003). Effective moment of inertia for glass fiber-reinforced polymer-reinforced concrete beams. *Structural Journal, 100*(6), 732-739.
21. Nanni, A., De Luca, A., & Zadeh, H. (2014). Reinforced concrete with FRP bars. Reinforced Concrete with FRP Bars. CRC Press, London, United Kingdom. *doi, 10*, b16669.
22. Benmokrane, B., Nazair, C., Seynave, X., & Manalo, A. (2017). Comparison between ASTM D7205 and CSA S806 tensile-testing methods for glass fiber–reinforced polymer bars. *Journal of Composites for Construction, 21*(5), 04017038.
23. Canadian Standards Association. (2002). *Design and construction of building components with fibre-reinforced polymers* (No. 2). Canadian Standards Association.
24. Kara, I. F., & Ashour, A. F. (2012). Flexural performance of FRP reinforced concrete beams. *Composite structures, 94*(5), 1616-1625.
25. Pecce, M., Manfredi, G., & Cosenza, E. (2000). Experimental response and code Modelsof GFRP RC beams in bending. *Journal of Composites for Construction, 4*(4), 182-190.
26. Shamass, R., & Cashell, K. A. (2020). Experimental investigation into the flexural behaviour of basalt FRP reinforced concrete members. *Engineering Structures, 220*, 110950.
27. Sijavandi, K., Sharbatdar, M. K., & Kheyroddin, A. (2021, October). Experimental evaluation of flexural behavior of high-performance fiber reinforced concrete beams using GFRP and high strength steel bars. In *Structures* (Vol. 33, pp. 4256-4268). Elsevier.
28. Xiao, S. H., Lin, J. X., Li, L. J., Guo, Y. C., Zeng, J. J., Xie, Z. H., ... & Li, M. (2021). Experimental study on flexural behavior of concrete beam reinforced with GFRP and steel-fiber composite bars. *Journal of Building Engineering, 43*, 103087.